J Sol-Gel Sci Technol (2015) 75:25–30
DOI 10.1007/s10971-015-3670-z

ORIGINAL PAPER

The synthesis of Cu_2ZnSnS_4 nanoparticles via an open-air solution route: influences of Zn precursor content

Jin Chen · Qinmiao Chen · Yi Ni · Yoshinori Yamaguchi · Tingting Wang · Zhen Jia · Xiaoming Dou · Songlin Zhuang

Received: 18 September 2014 / Accepted: 19 February 2015 / Published online: 5 March 2015

Abstract In the present work, Cu_2ZnSnS_4 (CZTS) nanoparticles (NPs) for use in low-cost thin film solar cells were successfully synthesized using a facile open-air solution route. Copper(II) chloride dihydrate, zinc(II) acetate dihydrate, tin(II) chloride, and thiourea were used as reagents, and oleylamine was employed as solvent. The effect of varying the Zn content in the precursor solution on the structural, morphological, compositional, and optical properties of the as-synthesized CZTS NPs was investigated via X-ray diffraction, scanning electron microscopy and transmission electron microscopy, energy dispersive X-ray spectroscopy and ultraviolet–visible–infrared spectroscopy, respectively. As observed, the properties of the as-synthesized NPs improved with increasing Zn precursor contents from 0.75 to 1.5 mmol. For instance, the crystallinity of the as-synthesized NPs improved gradually and the band gap energy was tuned from 1.28 to 1.41 eV. The Zn/Sn ratio increased from 0.51 to 0.86, whereas the Cu/(Zn + Sn) ratio decreased from 0.95 to 0.7 with increasing Zn precursor contents. The results indicated that the obtained CZTS NPs, prepared with a Zn precursor content of 1.5 mmol, are a good light-absorbing layer material for application in thin film solar cells.

Graphical Abstract

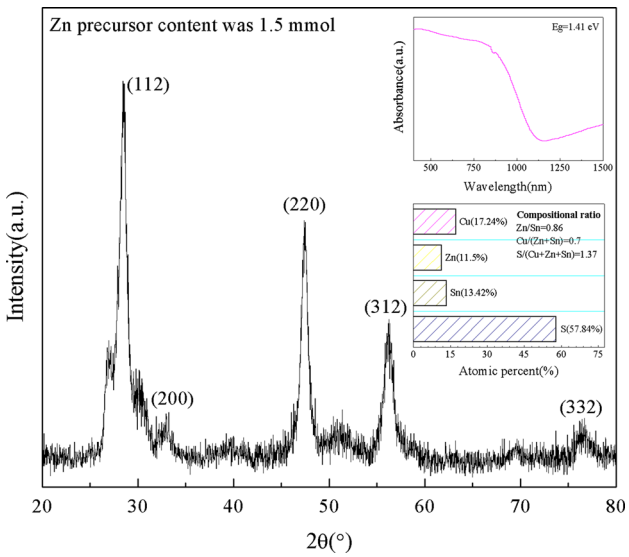

Keywords Cu_2ZnSnS_4 · Nanoparticles · Open-air solution route · Solar cells

1 Introduction

Recently, copper-based quaternary chalcopyrite Cu_2ZnSnS_4 (CZTS) semiconductor has spurred broad investigations as a

J. Chen · Q. Chen (✉) · Y. Ni · Y. Yamaguchi · T. Wang · Z. Jia · X. Dou
Department of Physics, College of Science, East China University of Science and Technology, 130 Meilong Road, Shanghai 200237, China
e-mail: jamechern@gmail.com

X. Dou
e-mail: xiaomingdou@yeah.net

J. Chen · T. Wang · Z. Jia · X. Dou · S. Zhuang
Engineering Research Center of Optical Instrument and System, Ministry of Education, Shanghai Key Lab of Modern Optical System, University of Shanghai for Science and Technology, Shanghai 200093, China

X. Dou
Consolidated Research Institute for Advanced Science and Medical Care, Waseda University, 513 Wasedatsurumaki-cho, Shinjuku-Ku, Tokyo 162-0041, Japan

promising absorbing layer candidate for application in low-cost thin film solar cells because of its high absorption coefficient ($>10^4$ cm^{-1}) and optimal band gap (1.0–1.5 eV) that are ideal properties for application under solar irradiation [1, 2]. Furthermore, all the constituent elements of CZTS are naturally abundant (Cu: 50 ppm, Zn: 75 ppm, Sn: 2.2 ppm, S: 260 ppm) and have low toxicity [3, 4]. Moreover, in contrast to the well-known absorber material $CuIn_xGa_{1-x}(S, Se)_2$ that constitutes rare and expensive In and Ga elements, CZTS consists of abundant and inexpensive Zn and Sn elements that are advantageous for the realization of low-cost solar cells. According to Shockley–Queisser photon balance calculations, CZTS-based solar cells can achieve a theoretical conversion efficiency of ~32.2 % [5]. Currently, the efficiency of CZTS-based solar cells is 12.6 %, as attained by the Mitzi group [6], who demonstrated that CZTS has great potential as an absorbing layer material for low-cost photovoltaic applications.

In previous studies, various approaches were developed for the fabrication of CZTS thin films, such as sputtering [7], thermal evaporation [8], pulsed laser deposition [9], electrochemical deposition [10], sol–gel method [11], spray pyrolysis [12], and ink printing [13]. Among these technologies, the ink printing route has attracted extensive attention owing to its excellent properties, e.g., simplicity, non-vacuum and low-temperature operating conditions, high material utilization efficiency (~100 %), and compatibility with roll-to-roll high-speed production processes. The synthesis of high-quality CZTS nanoparticles (NPs) for ink fabrication is the key step in this facile route. Several technologies have been employed for the synthesis of CZTS NPs such as hot-injection [14], solvothermal [15], and mechanochemical [16] methods. It is worth mentioning that Guo et al. [17] reported an efficiency of 7.2 % for solar cells based on CZTS NPs that were prepared by the hot-injection method. However, the hot-injection method, whereby precursors are injected into a hot organic medium to instigate the synthesis process, requires complex devices and an inert gas atmosphere. The solvothermal method also requires a complex reactor autoclave to achieve high pressures for the chemical reactions to proceed, as well as long reaction times, which is similar to the mechanochemical approach.

In the present work, CZTS NPs were synthesized via a facile and novel open-air solution approach. In contrast to previous methods, the current process was undertaken in an atmosphere ambient requiring no protecting gases, high pressures, or complex devices. To our knowledge, no similar reports have been reported to date. The influences of the Zn precursor content on the structural, compositional, optical, and morphological properties of the as-synthesized CZTS NPs were systematically investigated.

2 Experimental details

In a typical synthesis, 2 mmol copper(II) chloride dehydrate (AR from Sinopharm Chemical Reagent Co., Ltd), *n* (0.75, 1, 1.25, 1.5) mmol zinc(II) acetate dehydrate (AR from Sinopharm Chemical Reagent Co., Ltd), 1 mmol tin(II) chloride (AR from Sinopharm Chemical Reagent Co., Ltd), and 6 mmol thiourea (AR from Sinopharm Chemical Reagent Co., Ltd) (Cu:Zn:Sn:S = 2:*n*:1:6) were successively dissolved in 30 mL oleylamine (80–90 % from Aladdin), and the solution was stirred for 30 min at room temperature. A 100-mL three-neck round-bottom flask was employed as the vessel equipped with a reflux condenser. During stirring, the solution changed from sky blue to yellow–green. Then, the mixture was heated to 250 °C under open-air conditions and was maintained for 1 h to allow the NPs grow. The mixture color varied from yellow–green to brown–black while the temperature rose. Following completion of the reaction, the solution was allowed to cool to room temperature naturally. The black precipitate was collected from the solution by centrifugation (8000 rpm for 10 min) and washed with ethanol several times. Finally, the product was dried at 60 °C for several hours for characterization.

The crystal structure was determined by X-ray diffraction (XRD; MiniFlex 600, Rigaku) using Cu Kα radiation ($\lambda = 0.15406$ nm). The chemical composition was examined by energy dispersive X-ray spectroscopy (EDS; Genesis Apollo X, AMETEK). The morphology and microstructure of the NPs were investigated via field-emission scanning electron microscopy (FESEM; QUANTA FEG 450, FEI) and transmission electron microscopy (TEM; TECNAL G^2S-TWIN, FEI). The optical properties of the as-synthesized NPs were assessed using a reflection measurement route via ultraviolet–visible–infrared (UV–vis–IR) spectroscopy (Lambda 1050, PerkinElmer).

3 Results and discussion

The possible mechanism for the synthesis of the CZTS NPs using the current solution route is as follows. In the first step, the metal ions (Cu^{2+}, Zn^{2+}, Sn^{2+}) coordinate with thiourea (Tu) molecules to form Cu–Tu, Zn–Tu, and Sn–Tu complexes in solution. The formation of Cu–Tu complex is evident from the color change from sky blue (owing to free Cu^{2+}) to brown–black which indicates the disappearance of free Cu^{2+} ions. In the second stage, as the reaction proceeds, Tu reacts with trace water introduced by the solvent and hydrated metal salts to form H_2S. Concurrently, Cu–Tu is thermally decomposed into Cu^{2+} ions. Then, Cu^{2+} ions are reduced to Cu^+ by H_2S [18] and Sn^{2+} ions are oxidized to Sn^{4+} by Cu^{2+}. Finally, Cu^+, Zn^{2+},

Sn^{4+}, and S^{2-} ions organize themselves into crystal lattices to form CZTS.

To understand the variations in the NPs crystallite structure with changes in the Zn precursor content, the XRD patterns of the as-synthesized products are shown in Fig. 1a. The diffraction peaks at $2\theta \sim 28.4°$, 33.1°, 47.4°, 56.2°, and 76.6° were, respectively, attributed to the (112), (200), (220), (312), and (332) planes of kesterite CZTS (JCPDS 26-0575). The kesterite crystal structure is composed of a tetragonal unit cell whereby each sulfur anion is

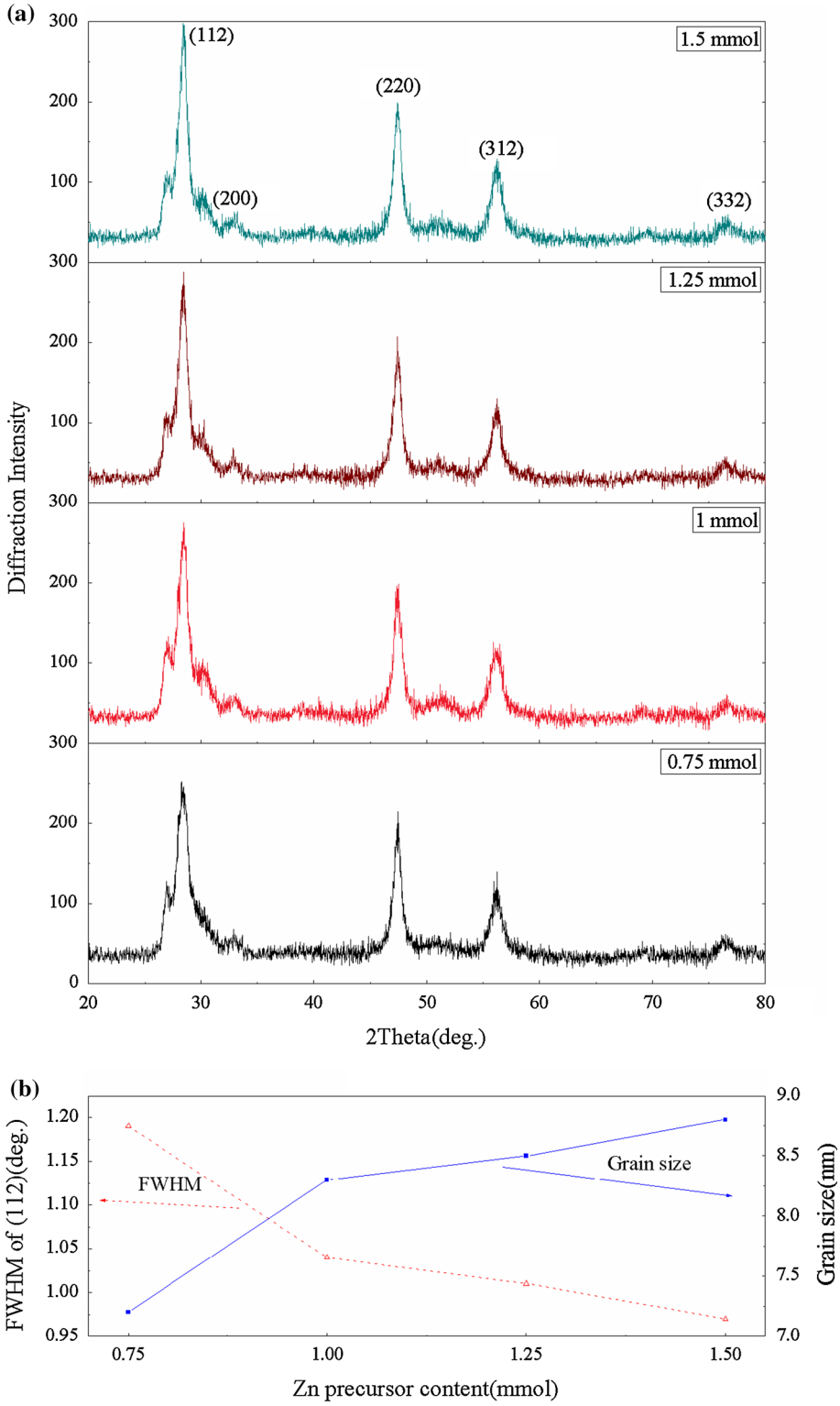

Fig. 1 **a** XRD patterns and **b** FWHM and grain size of the CZTS NPs prepared at varying Zn precursor contents

bonded to four cations and each cation is bonded to four sulfur anions, and the cation layers alternate with the sulfur anion layers along the c-axis as CuZn/SS/CuSn/SS [14]. As noted, the diffraction peaks became sharper with increasing Zn precursor contents from 0.75 to 1.5 mmol, indicating the growth of the CZTS NPs. Therefore, with increasing Zn precursor contents, more Zn could take part in the reaction, thereby promoting the growth of the NPs. Some impurity phases were additionally observed in the obtained products. The peaks at $2\theta \sim 26.8°$ and 30.2° were attributed to the binary sulfide phases $Cu_{2-x}S$ and SnS_2, respectively. The presence of impurities was most likely due to the non-vacuum operating conditions employed for the synthesis of the as-obtained products. A similar phenomenon was observed in a previous study [19]. Moreover, the presence of the secondary phases indicated the onset of Cu reduction and Sn oxidation reactions that further validate the CZTS NPs growth mechanism proposed above.

Figure 1b shows the variations in the full width at half maximum (FWHM) of the (112) peak and the mean crystallite size of the obtained products as a function of Zn precursor content. The crystallite size of the as-synthesized products was calculated using the Debye–Scherrer's formula: $D = k\lambda/\beta\cos\theta$, where D is the mean diameter of the crystallites, k is a constant, λ is the wavelength of Cu Kα (0.15406 nm), β is the FWHM of (112) peak, and θ is the diffraction angle. As observed, with increasing Zn precursor contents, the FWHM decreased from 1.19° to 0.97°. An opposite trend was observed for the mean crystallite size, which increased from 7.2 to 8.8 nm with increasing Zn precursor contents. The interplanar distance d and lattice constants a and c were calculated from the equation: $1/d^2 = 4\sin^2\theta/\lambda^2 = (h^2 + k^2)/a^2 + l^2/c^2$. At a Zn precursor content of 1.5 mmol, $d_{(112)}$ was ~ 3.14 Å, and a and c were 5.4214 and 10.9479 Å, respectively.

Figure 2a, b shows the variations in the atomic percent and compositional ratio of the as-obtained CZTS NPs as a function of Zn precursor content, respectively, as measured by EDS. As observed from Fig. 2a, the atomic content of Zn increased, as expected, with increasing Zn precursor contents from 0.75 to 1.5 mmol. Correspondingly, the content of Cu and Sn in the CZTS products decreased with increasing Zn contents. Accordingly, the ratio of Zn/Sn increased from 0.51 to 0.86 and that of Cu/(Zn + Sn) decreased from 0.95 to 0.7 with increasing Zn contents (Fig. 2b). As observed, when compared with elements Cu and Sn, Zn had the lowest reactivity rate, as noted in a previous report [20]. Higher Zn precursor contents enabled more Zn^{2+} to participate in the reaction, thereby addressing the low reactivity problem. In the Zn content range studied, a general upward trend in the S content was observed. A similar trend in the ratio of S/(Cu + Zn + Sn) was observed. Additionally, all the prepared NPs featured a high S content that could be attributed to the increasing amounts of S that were deliberately added to the precursor solution to ensure sufficient amounts of S for the growth of CZTS. When the Zn precursor content was 1.5 mmol, the ratios of Zn/Sn, Cu/(Zn + Sn), and S/(Cu + Zn + Sn) were 0.86, 0.7, and 1.37, respectively. As noted, the obtained CZTS NPs featured slightly Sn-rich that could be improved by annealing the fabricated CZTS film owing to the higher volatility of Sn when compared with that of Cu and Zn [21]. The low amount of Cu in the as-synthesized NPs is beneficial for fabricating optoelectronic devices with high efficiencies as suggested by an earlier work [22]. In summary, the above analysis suggests that a Zn precursor content of 1.5 mmol is

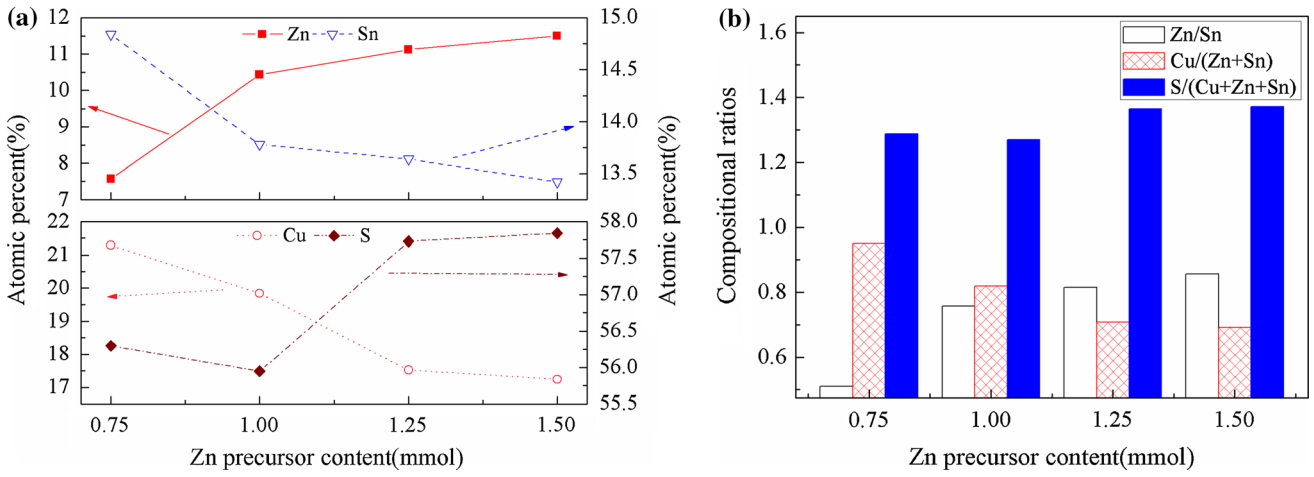

Fig. 2 Variations in the **a** atomic percent and **b** compositional ratio of the CZTS NPs as a function of Zn precursor content

ideal for preparing CZTS NPs of a suitable chemical composition for use in the fabrication of an absorber layer.

The optical properties of the as-synthesized NPs prepared with different Zn precursor contents were determined by UV–vis–IR spectroscopy and the results are shown in Fig. 3. The valence band of CZTS consists of an antibonding linear combination of Cu 3d and S 3p states, and the conduction band is dominated by an isolated band made up by Sn 5 s and S 3p states. Transitions from the Cu 3d/S 3p states to the conduction band determine the optical properties of the CZTS NPs in the visible region [23]. Figure 3a presents the absorption spectra of the obtained products. The absorbance values were recorded directly using a reflection measurement route, similar to that reported in Ref. [24]. The band gap energy of the samples was determined by extrapolating the straight line obtained from the plot of $(Ahv)^2$ as a function of hv, as shown in Fig. 3b, where A = absorbance, h = Planck's constant, and v = frequency [25]. The values of band gap energy of the as-synthesized NPs prepared at a Zn content of 0.75, 1, 1.25, and 1.5 mmol were 1.28, 1.32, 1.35, and 1.41 eV, respectively. As noted, the band gap energy increased with increasing Zn precursor contents. It is worth mentioning that the band gap energy of 1.41 eV obtained at a Zn precursor content of 1.5 mmol is comparable to the optimum value for photovoltaic solar conversion in single-band gap devices.

The above analysis indicated that a Zn precursor content of 1.5 mmol, when compared with the other Zn contents studied, was more advantageous for obtaining NPs properties (crystallinity, elemental composition, and optical feature) ideal for the fabrication of high-quality absorber layers. Figure 4 shows the morphology and microstructure of the NPs prepared at a Zn precursor content of 1.5 mmol, as examined by FESEM (Fig. 4a) and TEM (Fig. 4b, c), respectively. As depicted in Fig. 4a, the NPs featured an irregular spherical shape with a size of ~ 400–600 nm. As observed in Fig. 4b, the CZTS NPs were composed of small nanocrystals (NCs). The observed NPs from the NCs aggregation may be due to the high surface energy of the small CZTS NCs and the existence of van der Waals forces among the CZTS NCs [26, 27]. The NPs adopt a spherical configuration likely because such spherical structures possess the lowest surface energy [28]. As observed in Fig. 4b, the size of the NCs was calculated as 8–10 nm, which is consistent with the calculated value obtained from the XRD analysis. The high-resolution TEM image of an individual NC (Fig. 4c) shows clear lattice fringes with an interplanar distance of 3.14 Å that corresponds to the (112) plane, as consistent with the calculated value from the XRD analysis.

4 Conclusions

In summary, a novel open-air solution route, operating under an atmosphere ambient and requiring no protecting gases, high pressures, or complex devices, was reported for the facile synthesis of CZTS NPs. The effects of the Zn precursor content on the physical properties of the CZTS NPs, i.e., structural, compositional, optical, and morphological, were assessed by XRD, EDS, UV–vis–IR spectroscopy, and FESEM and TEM, respectively. The obtained CZTS NPs featured a kesterite structure, a suitable stoichiometry, and an irregular spherical shape. The particle size was ~400–600 nm, and the crystallite

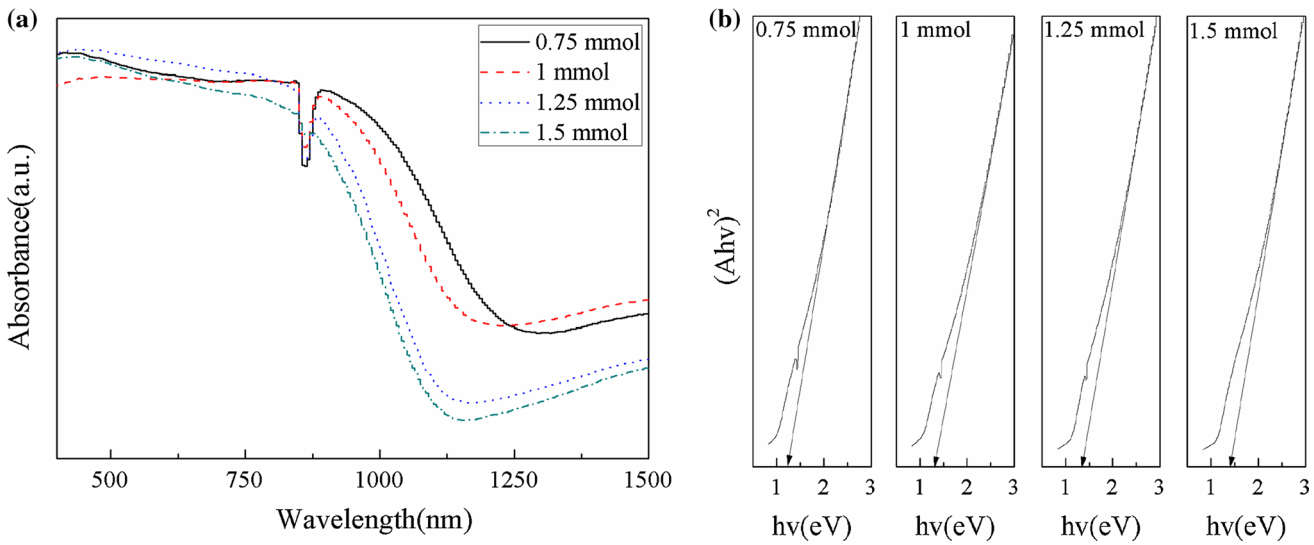

Fig. 3 **a** Absorption spectra and **b** *plots* of $(Ahv)^2$ as a function of hv of the CZTS NPs prepared at varying Zn precursor contents

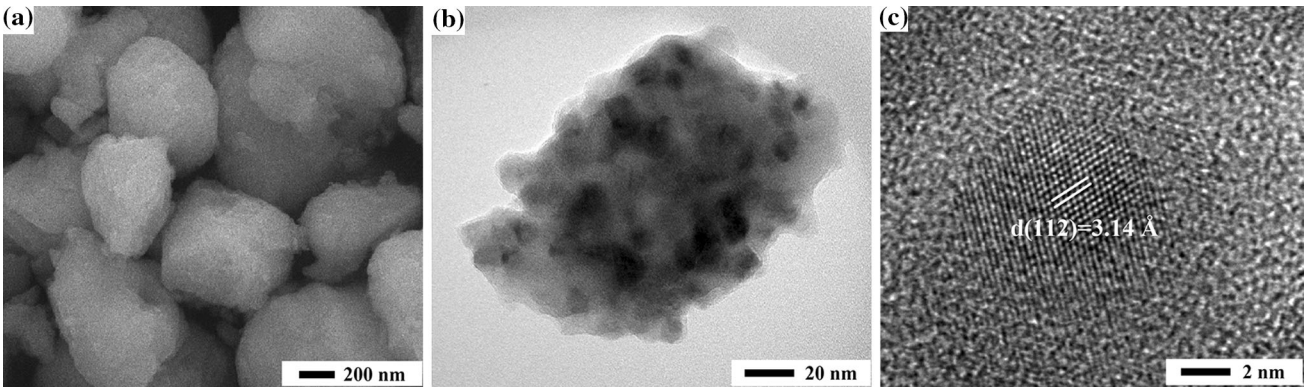

Fig. 4 **a** FESEM, **b** TEM, and **c** high-resolution TEM images of the as-synthesized CZTS (Zn content was 1.5 mmol)

diameter was ~ 8–10 nm. The band gap energy of the NPs was ~1.41 eV, which is optimal for photovoltaic applications. Further work will involve the fabrication of the CZTS NPs into a high-performance photovoltaic device.

Acknowledgments The project was financially supported by the Fundamental Re-search Funds for the Central Universities, China (No. WM1414047), Shanghai Committee of Science and Technology, China (No. 13JC1404300), Foundation for The Youth Scholars of Shanghai Municipal Education Commission, China (No. ZZSLG13013), Teachers' Innovation Ability Construction of University of Shanghai for Science and Technology, China (No. GDCX-Y-1205), Natural Science Foundation of Jiangsu Province, China (No. BK20141167), and Innovation Fund Project For Graduate Student of Shanghai, China (No. JWCXSL1301).

References

1. Shi L, Pei CJ, Xu YM, Li Q (2011) J Am Chem Soc 133:10328–10331
2. Kang CC, Chen HF, Yu TC, Lin TC (2013) Mater Lett 96:24–26
3. Chen J, Chen QM, Wang TT, Zhou FF, Jia Z, Dou XM, Zhuang SL (2014) Mater Lett 125:206–208
4. Katagiri H, Jimbo K, Maw WS, Oishi K, Yamazaki M, Araki H, Takeuchi A (2009) Thin Solid Films 517:2455–2460
5. Zhou J, You L, Li S, Yang Y (2012) Mater Lett 81:248–250
6. Wang W, Winkler MT, Gunawan O, Gokmen T, Todorov TK, Zhu Y, Mitzi DB (2013) Adv Energy Mater. doi:10.1002/aenm.201301465
7. Liu F, Li Y, Zhang K, Wang B, Yan C, Lai Y, Zhang Z (2010) Sol Energy Mat Sol C 94:2431–2434
8. Tanaka T, Yoshida A, Saiki D, Saito K, Guo Q, Nishio M, Yamaguchi T (2010) Thin Solid Films 518:S29–S33
9. Sun L, He J, Kong H, Yue F, Yang P, Chu J (2011) Sol Energy Mat Sol C 95:2907–2913
10. Chan CP, Lam H, Surya C (2010) Sol Energy Mat Sol C 94:207–211
11. Tanaka K, Fukui Y, Moritake N, Uchiki H (2011) Sol Energy Mat Sol C 95:838–842
12. Kamoun N, Bouzouita H, Rezig B (2007) Thin Solid Films 515:5949–5952
13. Chen QM, Dou XM, Li ZQ, Cheng SY, Zhuang SL (2011) Adv Mater Res 335:1406–1411
14. Guo Q, Hillhouse HW, Agrawal R (2009) J Am Chem Soc 131:11672–11673
15. Zhou Y, Zhou W, Du Y, Li M, Wu S (2011) Mater Lett 65:1535–1537
16. Wang Y, Gong H (2011) J Alloy Compd 509:9627–9630
17. Guo Q, Ford GM, Yang W, Walker BC, Stach EA, Hillhouse HW, Agrawal R (2010) J Am Chem Soc 132:17384–17386
18. Han S, Kong M, Guo Y, Wang M (2009) Mater Lett 63:1192–1194
19. Chen J, Chen QM, Yuan HC, Wang TT, Zhou FF, Dou XM, Zhuang SL (2014) J Mater Sci Mater Electron 25:873–881
20. Flynn B, Braly I, Glover PA, Oleksak RP, Durgan C, Herman GS (2013) Mater Lett 107:214–217
21. Byeon MR, Chung EH, Kim JP, Hong TE, Jin JS, Jeong ED, Bae JS (2013) Thin Solid Films 546:387–392
22. Chen SY, Gong XG, Walsh A, Wei SH (2010) Appl Phys Lett 96(2):021902
23. Paier J, Asahi R, Nagoya A, Kresse G (2009) Phys Rev B 79(11):115126
24. http://www.perkinelmer.com/Content/applicationnotes/app_uvvisnirmeasurebandgapenergyvalue.pdf
25. Zhao Y, Zhou W, Jiao J, Zhou Z, Wu S (2013) Mater Lett 96:174–176
26. Wang W, Shen HL, Jiang F, He XC, Yue ZH (2013) J Mater Sci Mater Electron 24:1813–1817
27. Wang Y, Liang X, Cai Q, Feng L, Shao M, Zhong J, Xiang W (2012) Acta Chim Sinica 70:903–910
28. Zhong LS, Hu JS, Liang HP, Cao AM, Song WG, Wan LJ (2006) Adv Mater 18:2426